Full-Parameter Omnidirectional Thermal Metadevices of Anisotropic Geometry

Tiancheng Han,* Peng Yang, Ying Li, Dangyuan Lei, Baowen Li, Kedar Hippalgaonkar, and Cheng-Wei Qiu*

Since the advent of transformation optics and scattering cancelling technology, a plethora of unprecedented metamaterials, especially invisibility cloaks, have been successfully demonstrated in various communities, e.g., optics, acoustics, elastic mechanics, dc electric field, dc magnetic field, and thermotics. A long-held captivation is that transformation-optic metamaterials of anisotropic or noncentrosymmetric geometry (e.g., ellipsoids) commonly come along with parameter approximation/simplification or directional functions. Here, a synthetic paradigm with strictly full parameters and omnidirectionality is reported simultaneously to address this long-held issue for molding heat flow and experimentally demonstrate a series of noncentrosymmetric thermal metadevices. It changes the usual perception that transformation thermotic/dc/acoustic metamaterials are just a direct and simplified derivatives of the transformation-optic counterpart. Instead, the proposed methodology solves an intriguingly important and challenging problem that is not possibly achievable for transformation-optic metamaterials. The approach is rigorous, exact, robust, and yet elegantly facile, which may open a new avenue to manipulating the Laplacian and wave-dynamic fields in ways previously inconceivable.

Prof. T. Han, P. Yang
School of Physical Science and Technology
Southwest University
Chongqing 400715, China
E-mail: tchan123@swu.edu.cn
Dr. Y. Li, Prof. C.-W. Qiu
Department of Electrical and Computer Engineering
National University of Singapore
4 Engineering Drive 3, Singapore 117583, Singapore
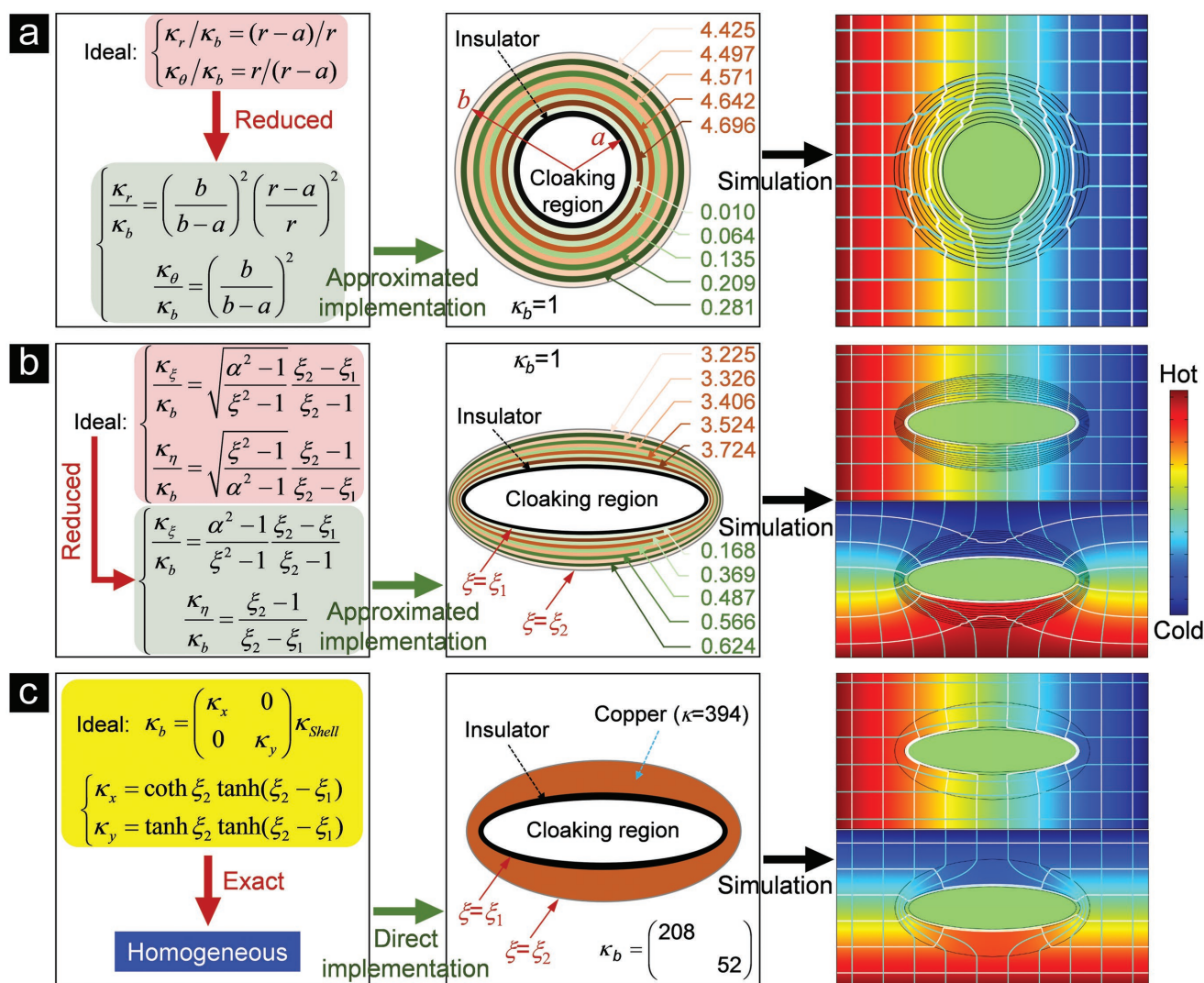E-mail: chengwei.qiu@nus.edu.sg
Prof. D. Lei
Department of Applied Physics
The Hong Kong Polytechnic University
Hong Kong 999077, China
Prof. B. Li
Department of Mechanical Engineering
University of Colorado
Colorado 80309, USA
Prof. K. Hippalgaonkar
Institute of Materials Research and Engineering
A*STAR, 2 Fusionopolis Way, Innovis, Singapore 138634, Singapore

Inspired by the pioneering theoretical works of transformation optics (TO)[1,2] and scattering cancelling technology,[3,4] a plethora of unprecedented devices, especially invisibility cloaks,[5–11] have been successfully demonstrated at various frequencies. The concept of invisible cloaking has attracted intensive research in various communities, e.g., optics,[12] far infrared,[13] acoustics,[14] elastic mechanics,[15,16] dc electric field,[17,18] dc magnetic field,[19,20] and thermotics.[21–24] A truly invisibility cloak should have full-parameters instead of reduced parameters and should be omnidirectional rather than unidirectional. However, the above two characteristics are often difficult to achieve simultaneously due to the extreme parameters (which are inhomogeneous, anisotropic, and singular).

As shown in **Figure 1**a, a circular thermal cloak can be designed with inhomogeneous and anisotropic conductivities expressed as $\kappa_r = \kappa_b(r - a)/r$ and $\kappa_\theta = \kappa_b r/(r - a)$, where κ_b is the thermal conductivity of background.[22] Obviously, κ_θ becomes infinity when $r \to a$. To avoid singularity, the parameters have to be simplified, which leads to a constant κ_θ and varied κ_r. Such a cloak ($a = 25$ mm and $b = 50$ mm) can be practically approximated utilizing a multilayered structure (we choose ten equally thick rings) with alternating large and small thermal conductivities.[23] Simulation result validates the design. Analogously, an elliptical thermal cloak can be designed in elliptical coordinate system (ξ, η) based on TO method, as demonstrated in Figure 1b. Obviously, the material parameters are also inhomogeneous, anisotropic, and singular (κ_ξ becomes infinity when $\xi \to 1$).[25] To avoid singularity, the parameters have to be simplified, which leads to a constant κ_η and varied κ_ξ. We note that $\alpha = (\xi - \xi_1)(\xi_2 - 1)/(\xi_2 - \xi_1) + 1$. For practical realization, such a cloak ($\xi_1 = 0.2793$ and $\xi_2 = 0.5494$) can be approximated with alternating large and small thermal conductivities. Simulation results show that a good performance is achieved in only one direction and no effect in other directions. This is because the expansion starts from a line segment rather than exactly from a point.[26] Though the omnidirectional elliptical cloak can be designed in theory, this, however, leads to extremely complicated parameters (which depend on both radius and angle).[27,28] To experimentally demonstrate a

**ADVANCED
SCIENCE NEWS**
www.advancedsciencenews.com
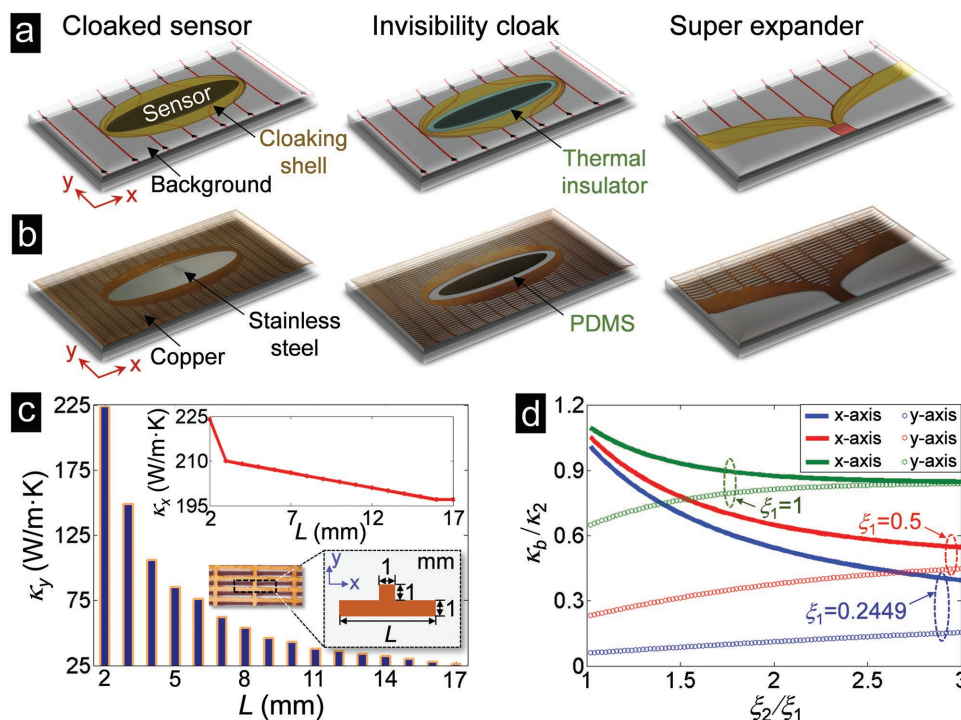
**ADVANCED
MATERIALS**
www.advmat.de

Figure 1. Material parameters, implementation strategies, and simulation results for: a) the TO-based circular cloak, b) elliptical cloak, and c) the proposed full-parameter omnidirectional elliptical cloak. Obviously, the TO-based cloaks require inhomogeneous, anisotropic, and singular material parameters, which has to be reduced for experimental realization. Though complicated multilayers are employed to realize the elliptical cloak, it functions in only one direction and no effect in other directions. In contrast, our scheme demonstrates great advantages, including approximation-free homogeneous parameters, extremely simple implementation employing only one layer of natural bulk material, and excellent performance for arbitrary heat launching angles. It is noted that the unit of thermal conductivity κ is W m^{-1} K^{-1}. Isothermal lines (white) and streamlines (light blue) are also represented in the third column panel.

full-parameter omnidirectional cloak of irregular noncentrosymmetric geometry is a task usually considered to be "a mission impossible."

Here, we demonstrate the design of full-parameter omnidirectional thermal metadevices with anisotropic geometry, which is experimentally confirmed via three proof-of-concept experiments (viz., a cloaked sensor, invisibility cloak, and a super expander). Compared to the TO-based thermal cloaks in Figure 1a,b, the proposed scheme in Figure 1c, derived directly from the conduction equation, demonstrates great advantages, including exact design with approximation-free homogeneous parameters, plausible implementation with homogenous and isotropic natural bulk materials, and excellent performance along arbitrary directions of heat flow. The remarkable

performance has been verified in the time dependent case as well, indicating excellent thermodynamic performance. Our method is applicable not only to thermal cloak,[29–32] but also to dc magnetic cloak[33–36] and dc electric cloak.[37]

We start with the concept of a cloaked sensor,[38] which is capable of cloaking itself and still receiving an incoming signal simultaneously. An exposed sensor can be identified due to its unique scattering signature. When an elliptical sensor is wrapped by a conformal shell, the severely deformed heat flux restores exactly without distortion as if nothing were there, as demonstrated in the left panel of **Figure 2**a. Without loss of generality, we carry on a rigorous analysis in the elliptical coordinate system (ξ, η). We consider an elliptical sensor of boundary ξ_1 wrapped by a shell of interior and exterior boundaries ξ_1 and

**ADVANCED
SCIENCE NEWS**

www.advancedsciencenews.com

**ADVANCED
MATERIALS**

www.advmat.de

Figure 2. Evolution, function, and realization from a cloaked sensor to super expander. a) Function demonstration of cloaked sensor, invisibility cloak, and super expander, in which the heat flux distributions are illustrated by the red lines. b) Photos of the fabricated cloaked sensor, invisibility cloak, and super expander, respectively. c) The thermal conductivity along the *y*-axis of the designed anisotropic material varying with period L. The upper inset shows the thermal conductivity along the *x*-axis varying with period L. The lower inset shows the unit cell of the designed anisotropic material. d) κ_b/κ_2 as a function of ξ_2/ξ_1, when ξ_1 is equal to 0.2449, 0.5, and 1, respectively. The solid lines and the open circles correspond to the thermal conductivities along the *x*-axis and along *y*-axis, respectively.

ξ_2. It is remarked that the inner and outer ellipses are of the same focus. The thermal conductivities of the sensor, shell, and background are κ_1, κ_2, and κ_b, respectively. We first consider a uniform heat flux externally applied in the *x*- direction. In the limit where the external temperature-field distortion is completely eliminated, we obtain

$$\kappa_b = \kappa_2 Q_1 \coth \xi_2 \qquad (1)$$

where $Q_1 = \dfrac{\kappa_1 \sinh \xi_1 \cosh(\xi_2 - \xi_1) + \kappa_2 \cosh \xi_1 \sinh(\xi_2 - \xi_1)}{\kappa_1 \sinh \xi_1 \sinh(\xi_2 - \xi_1) + \kappa_2 \cosh \xi_1 \cosh(\xi_2 - \xi_1)}$.

Analogously, when a uniform heat flux is externally applied in the *y* direction, we obtain

$$\kappa_b = \kappa_2 Q_2 \tanh \xi_2 \qquad (2)$$

where $Q_2 = \dfrac{\kappa_1 \cosh \xi_1 \cosh(\xi_2 - \xi_1) + \kappa_2 \sinh \xi_1 \sinh(\xi_2 - \xi_1)}{\kappa_1 \cosh \xi_1 \sinh(\xi_2 - \xi_1) + \kappa_2 \sinh \xi_1 \cosh(\xi_2 - \xi_1)}$.

Rigorous analysis is provided in the Supporting Information. Considering that the sensor (central region) and cloaking shell are stainless steel 304 (with $\kappa = 16$ W m^{-1} K^{-1}) and copper (with $\kappa = 394$ W m^{-1} K^{-1}), respectively, the thermal conductivities of the background are determined accurately by Equations (1) and (2). The performance of the proposed cloaking elliptical sensor has been numerically confirmed in Figure S1 in the Supporting Information. We remark that the length of major axis for outer ellipse of the shell is always chosen as $a_2 = 50$ mm, either for simulations or experiments.

From Equations (1) and (2), we know that the background material is generally anisotropic for an elliptical device. Here, we implement the anisotropic background material with a periodic structure of a T-shaped unit, as demonstrated in the lower inset of Figure 2c. The base material is copper plate with thickness of 1 mm. With the change of period L, the background thermal conductivity along the *y*-direction is illustrated in Figure 2c. It is seen that κ_y may reach as small as 26 W m^{-1} K^{-1} when $L = 17$ mm. The background thermal conductivity along the *x*-direction is also varied with the period L, as demonstrated in the upper inset of Figure 2c. However, κ_x becomes a constant of 197 W m^{-1} K^{-1} when L is large enough and that can be well interpreted with effective medium theory. In this instance, the structure can be regarded as multilayers with alternating copper and air, thus leading to $\kappa_x = \kappa_{\text{copper}}/2$.

The experimental realization of a cloaked elliptical sensor is illustrated in the left panel of Figure 2b, in which the sensor (central region) and cloaking shell are stainless steel 304 and copper, respectively. We choose $\xi_1 = 0.2449$ and $\xi_2 = 0.4516$, thus leading to the background thermal conductivities of $\kappa_x = 198$ W m^{-1} K^{-1} and $\kappa_y = 60$ W m^{-1} K^{-1}. Accordingly, we choose $L = 8$ mm and the dimension of the background as 161 mm × 83 mm. To reduce the heat convection by air as well as the high reflection by copper, a thin polydimethylsiloxane (PDMS) ($\kappa = 0.15$ W m^{-1} K^{-1}) film (≈0.1 mm) is deposited on the surface of each sample. In the experimental setup, local heating on one side of the plate is achieved by a heat source fixed at 70 °C, while the other side is connected to a tank filled
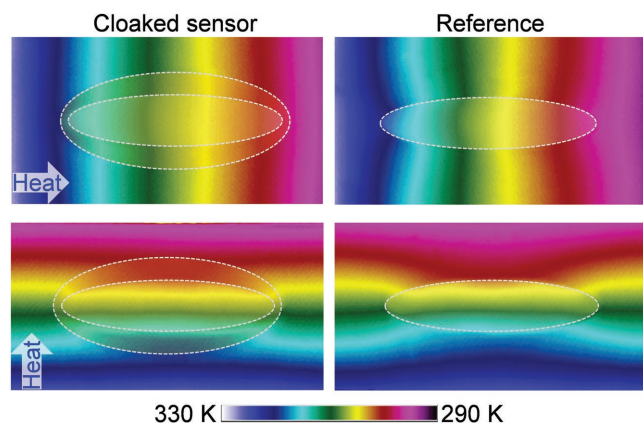
Figure 3. Measured temperature profiles for cloaked sensor and reference structure (a bare sensor) in steady state.

with ice water (0 °C). The cross-sectional temperature is captured with an optris PI400 infrared camera.

For comparison, we also fabricated a reference structure that is a bare sensor without cloaking shell (parameters like those for the cloaking sensor). **Figure 3** shows the measured temperature profiles for cloaked sensor and reference structure in steady state. We can see that the cloaked sensor successfully fulfills its task in that the sensor is capable of receiving an incoming signal (since the heat flows through the sensor) without distorting the external temperature field. Furthermore, both front and rear temperature fronts outside the cloaked sensor remain planar. In contrast, the bare sensor completely alters the temperature profile, which allows the sensor to be detected.

A cloaked sensor has to change the shell when either the material or geometrical size of the sensor is changed, which can be found in Equations (1) and (2). Actually, in most instances, an object only needs to be rendered invisible without receiving the incoming signal. When an insulating layer is located between the object and cloaking shell, heat flux may be prevented from touching the object. We thus derive an invisibility cloak, as conceptually demonstrated in the middle panel of Figure 2a. By setting $\kappa_1 = 0$, we can obtain the relationship for invisibility cloak from Equations (1) and (2). When a uniform heat flux is externally applied in the x direction, invisibility cloak satisfies

$$\kappa_b = \kappa_2 \coth \xi_2 \tanh (\xi_2 - \xi_1) \tag{3}$$

When a uniform heat flux is externally applied in the y direction, invisibility cloak satisfies

$$\kappa_b = \kappa_2 \tanh \xi_2 \tanh (\xi_2 - \xi_1) \tag{4}$$

Hence, an exact elliptical cloak, derived directly from the thermal conduction equation $\nabla \cdot (\kappa \nabla T) = 0$, has been obtained. Equations (3) and (4) represent a whole family of solutions for an elliptical cloak, depending on κ_b/κ_2, ξ_2/ξ_1, and ξ_1, which are calculated in Figure 2d. Therefore, we can see that an elliptical cloak generally requires an anisotropic background. However, when $\xi_1 = 1$, the background becomes isotropic as long as ξ_2/ξ_1 is not smaller than 3, which corresponds to a

nearly perfect circular cloak.[32] Considering that the object and cloaking shell are stainless steel 304 and copper, respectively, an insulating layer is placed between the object and cloaking shell. The performance of the proposed bilayer elliptical cloak has been numerically confirmed in Figure S2 in the Supporting Information.

Now, moving on to the consideration of transient states, the governing equation is $\rho c \frac{\partial T}{\partial t} - \nabla \cdot (\kappa \nabla T) = 0$, whose solution depends on the thermal diffusivity $\kappa / \rho c$. Therefore, if $\kappa / \rho c$ for the shell and background are equal, i.e., $\kappa / \rho c = $ constant, the proposed elliptical cloak may have excellent performance in the transient case. To confirm this point, we consider an elliptical cloak with $\xi_1 = 0.2449$ and $\xi_2 = 0.469$, thus leading to background thermal conductivities of $\kappa_x = 198$ W m^{-1} K^{-1} and $\kappa_y = 38$ W m^{-1} K^{-1}. The product ρc of the copper shell is $\rho c = 3.4$ MJ m^{-3} K^{-3}. In Figure S3 in the Supporting Information, it is clearly seen that the transient performance of the elliptical cloak is outstanding when $\kappa / \rho c = $ constant is satisfied for both shell and background materials. However, when $\kappa / \rho c$ is not a constant in shell and background materials, good performance can only be achieved after a relatively long time. The proposed scheme (drilling holes in the copper plate) satisfies $\kappa / \rho c = $ constant well since the thermal conductivity κ and product ρc of air can be neglected compared to the copper.

We next experimentally realize the elliptical cloak illustrated in the middle panel of Figure 2b, in which the shell is copper, and an insulating layer (PDMS) is located between the cloaking object and shell. The required thermal conductivities of the background are satisfied when $L = 11$ mm. The dimension of the fabricated sample is 155 mm × 83 mm. For comparison, we have also fabricated a reference structure in which the object is covered by a single layer of PDMS (parameters like those for the cloak). **Figure 4** shows the transient temperature distributions of the elliptical cloak and reference structure at different times, $t = 0.5, 1, 2,$ and 5 min after touching the heat source. Figure 4a,c corresponds to the invisibility cloak when heat flows along the x direction and the y direction, respectively. Figure 4b,d corresponds to the reference structure when heat flows along the x direction and the y direction, respectively. Obviously, the isothermal lines near the reference structure are significantly curved. When the perturbation is wrapped by the proposed cloak, the curved isothermal lines restore exactly without distortion as if nothing were there. As time elapses, our elliptical cloak is always able to successfully fulfill its objective, demonstrating excellent transient performance.

The proposed elliptical cloak also has excellent performance under an oblique heat flux direction, as is demonstrated in **Figure 5**a. It is clearly seen that the elliptical cloak performs as perfectly as the background without any distortion, showing much better performance compared to the reference structure. It is noted that the anisotropy of the background increases with the increase of the eccentricity (which is defined as the ratio of focal length p to major axis a_1) of an elliptical cloak. However, when the eccentricity of a bilayer cloak is not too large (e.g., $p/a_1 \leq 1/2$), the anisotropic background may be replaced with an isotropic material with a pretty good performance. For example, we consider an elliptical cloak with $p/a_1 = 1/2$ and $p/a_2 = 5/12$, resulting in an anisotropic background of $\kappa_b = \begin{pmatrix} 88 & 0 \\ 0 & 72 \end{pmatrix}$. When the small anisotropy is neglected ($\kappa_b = 80$ W m^{-1} K^{-1}), a fairly
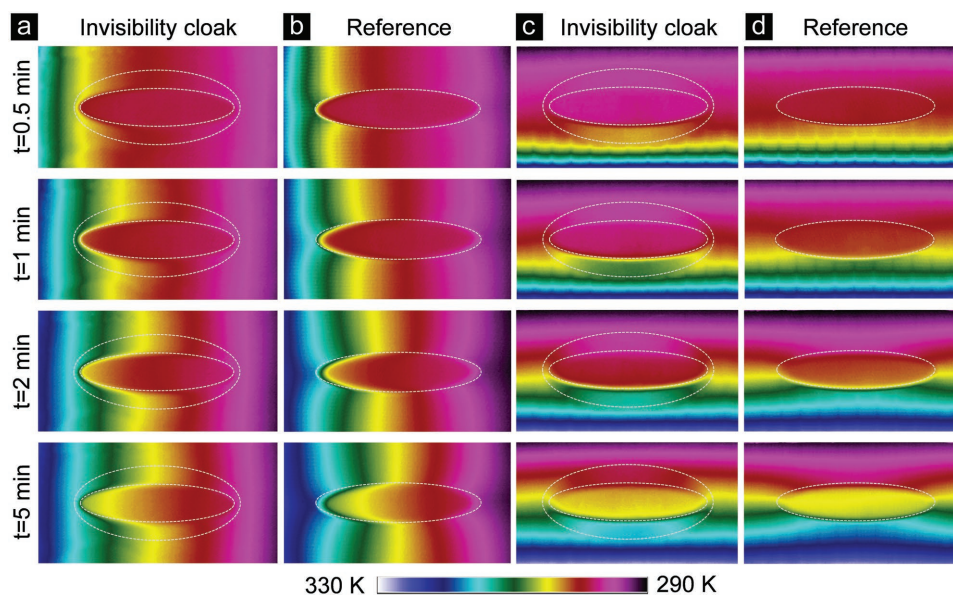
Figure 4. Measured transient temperature profiles for the invisibility cloak and reference structure (with only a thermally insulating ring around the central cloaking region) at different times $t = 0.5$, 1, 2, and 5 min. a) Results for the invisibility cloak when the heat flows from left to right. b) Results for the reference structure when the heat flows from left to right. c) Results for the invisibility cloak when the heat flows from bottom to top. d) Results for the reference structure when the heat flows from bottom to top.

good performance is obtained with arbitrary incoming heat flux angles, as illustrated in Figure 5b.

Inspired by the elliptical cloak, a super thermal expander, which acts as an ultrahigh-efficiency point-to-plane heat source convertor, can be naturally constructed, as conceptually demonstrated in the right panel of Figure 2a. When the shell is chosen as copper, the background thermal conductivity is determined

by geometrical size according to Equation (4). The performance of the proposed super thermal expander has been numerically confirmed in Figure S4 in the Supporting Information. Different from the previous scheme utilizing inhomogeneous and anisotropic metamaterials that are challenging to fabricate,[39] our scheme only utilizes a layer of natural bulk material. Compared with the scheme in which the ratio of width to height is always kept as 2,[40] our scheme could approach infinity in principle, demonstrating much more compact and efficient advantageous.

We experimentally realize the super expander illustrated in the right panel of Figure 2b, which is a direct evolution from the design of the elliptical cloak. Local heating on the narrow side of the expander is achieved by a point heat source fixed at 70 °C, while the wide side is connected to a tank filled with water at room temperature. The transient temperature distributions are measured at different times $t = 0.5$, 1, 2, and 5 min after touching the heat source, as demonstrated in **Figure 6**a. Obviously, the temperature fronts of the super expander remain planar as time elapses, demonstrating an ultrahigh-efficiency point-to-plane conversion and excellent transient performance. For comparison, we have fabricated a corresponding reference structure in which the shell is replaced by the background (parameters like those for the super expander). The transient temperature distributions of the reference structure are also demonstrated in Figure 6b, demonstrating cylindrical heat fronts. Obviously, with our super expander,
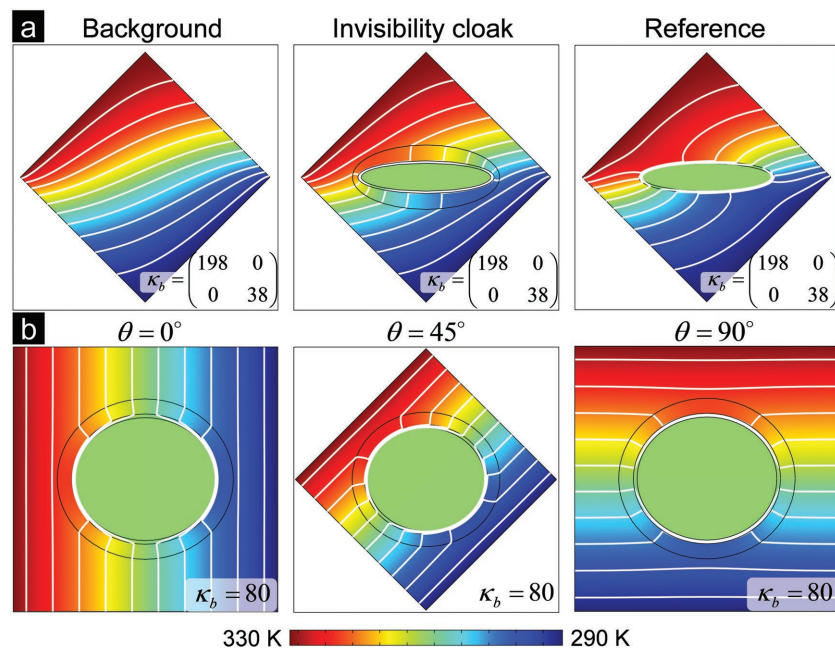
Figure 5. a) Simulated temperature distributions of the background, invisibility cloak, and reference structure under heat launching angle of 45°. b) Simulated temperature distributions of an elliptical cloak with $p/a_1 = 1/2$ and $p/a_2 = 5/12$ under different incoming heat flux angles of $\theta = 0°$, 45°, and 90°. Isothermal lines are also represented with white color in the panel.
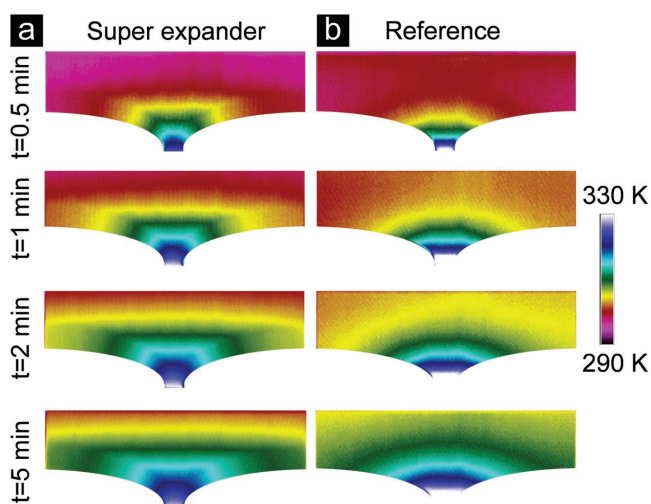
Figure 6. Measured transient temperature profiles for super expander and reference structure at different times *t* = 0.5, 1, 2, and 5 min, when a point source is located at the bottom. a) Results for the super expander. b) Results for the reference structure.

the cylindrical temperature fronts have been successfully rectified to be planar, demonstrating much better performance compared to other recently proposed schemes.[39,40]

In summary, we experimentally demonstrate full manipulation of heat flux in thermal metadevices with irregular boundaries (viz., a cloaked sensor, invisibility cloak, and a super expander) that make no approximation in any parameters. Our design schemes—derived rigorously from thermal conduction equation—are exact rather than approximate ones, thus avoiding extreme material parameters and complicated fabrication. In addition, the proposed schemes are implemented with existing natural bulk materials, thus indicating that our advanced scheme is ready for real engineering applications. Our approach may provide a more general platform for thermal camouflage,[41,42] multiphysics cloak,[43,44] multiphysics cloaking sensor,[45] and thermal diodes.[46]

Supporting Information

Supporting Information is available from the Wiley Online Library or from the author.

Acknowledgements

Conflict of Interest

The authors declare no conflict of interest.

[1] J. B. Pendry, D. Schurig, D. R. Smith, *Science* **2006**, *312*, 1780.
[2] U. Leonhardt, *Science* **2006**, *312*, 1777.
[3] A. Alù, N. Engheta, *Phys. Rev. E* **2005**, *72*, 016623.
[4] A. Alù, N. Engheta, *Phys. Rev. Lett.* **2008**, *100*, 113901.
[5] R. Peng, Z. Xiao, Q. Zhao, F. Zhang, Y. Meng, B. Li, J. Zhou, Y. Fan, P. Zhang, N. Shen, T. Koschny, C. M. Soukoulits, *Phys. Rev. X* **2017**, *7*, 011033.
[6] B. Zheng, H. A. Madni, R. Hao, X. Zhang, X. Liu, E. Li, H. Chen, *Light: Sci. Appl.* **2016**, *5*, e16177.
[7] N. Landy, D. R. Smith, *Nat. Mater.* **2013**, *12*, 25.
[8] X. Ni, Z. Wong, M. Mrejen, Y. Wang, X. Zhang, *Science* **2015**, *349*, 1310.
[9] Y. Yang, L. Jing, B. Zhang, R. Hao, W. Yin, E. Li, C. M. Soukoulis, H. Chen, *Adv. Mater.* **2016**, *28*, 6866.
[10] S. Xu, X. Chen, S. Xi, R. Zhang, H. O. Moser, Z. Shen, Y. Xu, Z. Huang, X. Zhang, F. Yu, B. Zhang, H. Chen, *Phys. Rev. Lett.* **2012**, *109*, 223903.
[11] D. Schurig, J. J. Mock, B. J. Justice, S. A. Cummer, J. B. Pendry, A. F. Starr, D. R. Smith, *Science* **2006**, *314*, 977.
[12] H. Chen, B. Zheng, L. Shen, H. Wang, X. Zhang, N. I. Zheludev, B. Zhang, *Nat. Commun.* **2013**, *4*, 3652.
[13] L. Shen, B. Zheng, Z. Liu, Z. Wang, S. Lin, S. Dehdashti, E. Li, H. Chen, *Adv. Opt. Mater.* **2015**, *112*, 7635.
[14] S. Zhang, C. Xia, N. Fang, *Phys. Rev. Lett.* **2011**, *106*, 024301.
[15] M. Farhat, S. Guenneau, S. Enoch, *Phys. Rev. Lett.* **2009**, *103*, 024301.
[16] N. Stenger, M. Wilhelm, M. Wegener, *Phys. Rev. Lett.* **2012**, *108*, 014301.
[17] F. Yang, Z. Mei, T. Jin, T. Cui, *Phys. Rev. Lett.* **2012**, *109*, 053902.
[18] W. Jiang, C. Luo, Z. Mei, T. Cui, *Appl. Phys. Lett.* **2013**, *102*, 014102.
[19] B. Wood, J. B. Pendry, *J. Phys.: Condens. Matter* **2007**, *19*, 076208.
[20] F. Magnus, B. Wood, J. Moore, K. Morrison, G. Perkings, J. Fyson, M. C. K. Wiltshire, D. Caplin, L. F. Cohen, J. B. Pendry, *Nat. Mater.* **2008**, *7*, 295.
[21] C. Fan, Y. Gao, J. Huang, *Appl. Phys. Lett.* **2008**, *92*, 251907.
[22] S. Guenneau, C. Amra, D. Veynante, *Opt. Express* **2012**, *20*, 8207.
[23] R. Schittny, M. Kadic, S. Guenneau, M. Wegener, *Phys. Rev. Lett.* **2013**, *110*, 195901.
[24] Y. Ma, L. Lan, W. Jiang, F. Sun, S. He, *NPG Asia Mater.* **2013**, *5*, e73.
[25] X. Yuan, G. Lin, Y. Wang, *Int. J. Mod. Phys. B* **2017**, *31*, 1650244.
[26] W. X. Jiang, T. J. Cui, G. X. Yu, X. Q. Lin, Q. Cheng, J. Y. Chin, *J. Phys. D: Appl. Phys.* **2008**, *41*, 085504.
[27] H. Ma, S. Qu, Z. Xu, J. Zhang, B. Chen, J. Wang, *Phys. Rev. A* **2008**, *77*, 013825.
[28] W. X. Jiang, T. J. Cui, X. M. Yang, Q. Cheng, R. Liu, D. R. Smith, *Appl. Phys. Lett.* **2008**, *93*, 194102.
[29] S. Narayana, Y. Sato, *Phys. Rev. Lett.* **2012**, *108*, 214303.
[30] T. Han, T. Yuan, B. Li, C.-W. Qiu, *Sci. Rep.* **2013**, *3*, 1593.
[31] H. Xu, X. Shi, F. Gao, H. Sun, B. Zhang, *Phys. Rev. Lett.* **2014**, *112*, 054301.
[32] T. Han, X. Bai, D. Gao, J. T. L. Thong, B. Li, C.-W. Qiu, *Phys. Rev. Lett.* **2014**, *112*, 054302.
[33] S. Narayana, Y. Sato, *Adv. Mater.* **2012**, *24*, 71.

[34] F. Gömöry, M. Solovyov, J. Šouc, C. Navau, J. Part-Camps, A. Sanchez, *Science* **2012**, *335*, 1466.

[35] J. Zhu, W. Jiang, Y. Liu, G. Yin, J. Yuan, S. He, Y. Ma, *Nat. Commun.* **2015**, *6*, 8931.

[36] W. Jiang, Y. Ma, J. Zhu, G. Yin, Y. Liu, J. Yuan, S. He, *NPG Asia Mater.* **2017**, *9*, e341.

[37] T. Han, H. Ye, Y. Luo, S. P. Yeo, J. Teng, S. Zhang, C.-W. Qiu, *Adv. Mater.* **2014**, *26*, 3478.

[38] A. Alù, N. Engheta, *Phys. Rev. Lett.* **2009**, *102*, 233901.

[39] Y. Liu, W. Jiang, S. He, Y. Ma, *Opt. Express* **2014**, *22*, 170006.

[40] R. Wang, L. Xu, J. Huang, *J. Appl. Phys.* **2017**, *122*, 215107.

[41] T. Han, X. Bai, J. T. L. Thong, B. Li, C.-W. Qiu, *Adv. Mater.* **2014**, *26*, 1731.

[42] R. Hu, S. Zhou, Y. Li, D. Lei, X. Luo, C.-W. Qiu, *Adv. Mater.* **2018**, *30*, 1707237.

[43] Y. Ma, Y. Liu, M. Raza, Y. Wang, S. He, *Phys. Rev. Lett.* **2014**, *113*, 205501.

[44] Y. Yang, H. Wang, F. Yu, Z. Xu, H. Chen, *Sci. Rep.* **2016**, *6*, 20219.

[45] T. Yang, X. Bai, D. Gao, L. Z. Wu, B. W. Li, J. T. L. Thong, C. W. Qiu, *Adv. Mater.* **2015**, *27*, 7752.

[46] Y. Li, X. Shen, Z. Wu, J. Huang, Y. Chen, Y. Ni, J. Huang, *Phys. Rev. Lett.* **2015**, *115*, 195503.